Convolution Filter based Efficient Multispectral Image Demosaicking for Compact MSFAs

Vishwas Rathi[a] and Puneet Goyal[b]
Department of Computer Science and Engineering, Indian Institute of Technology Ropar, Rupnagar, Punjab, India

Keywords: Demosaicking, Multispectral Filter Array, Interpolation, Multispectral Image, Convolution Filter.

Abstract: Using the multispectral filter arrays (MSFA) and demosaicking, the low-cost multispectral imaging systems can be developed that are useful in many applications. However, multispectral image demosaicking is a challenging task because of the very sparse sampling of each spectral band present in the MSFA. The selection of MSFA is very crucial for the applicability and for the better performance of demosaicking methods. Here, we consider widely accepted and preferred MSFAs that are compact and designed using binary tree based approach and for these compact MSFAs, we propose a new efficient demosaicking method that relies on performing filtering operations and can be used for different bands size multispectral images. We also present new filters for demosaicking based on the probability of appearance of spectral bands in binary-tree based MSFAs. Detailed experiments are performed on multispectral images of two different benchmark datasets. Experimental results reveal that the proposed method has wider applicability and is efficient; it consistently outperforms the existing state-of-the-art generic multispectral image demosaicking methods in terms of different image quality metrics considered.

1 INTRODUCTION

Standard color image cameras capture the scene's information in only three bands (Red, Green, and Blue) of electromagnetic spectrum. However, a multispectral image has more than three spectral bands, which makes the multispectral image more informative about the scene than the standard color image. Therefore, multispectral imaging is discovered valuable in many research areas, for example, remote sensing, medical imaging, food industry, and computer vision (MacLachlan et al., 2017; Pichette et al., 2016; Qin et al., 2013; Liu et al., 2014; Zia et al., 2015; Chen and Lin, 2020; Vayssade et al., 2020; Zenteno et al., 2019; Junior et al., 2019). Contingent upon the application, there is an alternate prerequisite of data to be caught. These numerous prerequisites in various space inspired the manufacturer to develop multispectral imaging (MSI) systems (Fukuda et al., 2005; Thomas et al., 2016; Geelen et al., 2014; Martinez et al., 2014; Shrestha et al., 2011; Tsuchida et al., 2012; Pichette et al., 2016; Ohsawa et al., 2004; Monno et al., 2015) of varying spectral bands.

[a] https://orcid.org/0000-0002-6770-6142
[b] https://orcid.org/0000-0002-6196-9347

In the last few years, different MSI systems have been proposed with different techniques to capture the multispectral image. These systems can be divided into three distinctive categories (Monno et al., 2011): (i) Multi-Camera-One-Shot systems (Ohsawa et al., 2004; Shrestha et al., 2011), which capture images utilizing a few cameras with various spectral bands in a single shot, bringing about a framework that is very confounded as it requires proper arrangement of different cameras, and these systems are expensive as they utilize various cameras. (ii) Single-Camera-Multi-Shot systems (Fukuda et al., 2005; Chi et al., 2010), which are used by changing the color filter array in front of the imaging sensor or by changing the lighting source. These requirements restrict the video capturing using these systems. (iii) Single-Camera-One-Shot systems (Thomas et al., 2016; Geelen et al., 2014; Martinez et al., 2014; Monno et al., 2015), similar to standard RGB cameras, which overcome the issues of the first two categories of systems in terms of cost, size, and video capturing.

The standard RGB camera uses a single sensor to capture three bands' information with a color filter array (CFA), where only one-pixel value among RGB values is captured at each pixel location. This captured mosaic data is called the CFA image, and the

Rathi, V. and Goyal, P.
Convolution Filter based Efficient Multispectral Image Demosaicking for Compact MSFAs.
DOI: 10.5220/0010249601120121
In *Proceedings of the 16th International Joint Conference on Computer Vision, Imaging and Computer Graphics Theory and Applications (VISIGRAPP 2021) - Volume 4: VISAPP*, pages 112-121
ISBN: 978-989-758-488-6

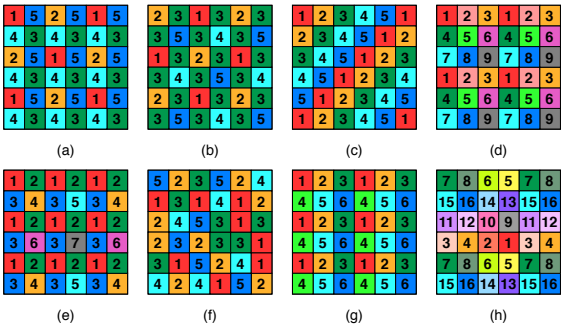

Figure 1: MSFA designs. (a) BTES (Miao and Qi, 2006), (b) Monno (Monno et al., 2015), (c) Uniform (Aggarwal and Majumdar, 2014b), (d) Square(Non-redundant) (Mihoubi et al., 2015), (e) GAP (Yasuma et al., 2010), (f) Random (Aggarwal and Majumdar, 2014a), (g) Brauers (Brauers and Aach, 2006), (h) IMEC (Geelen et al., 2014).

process of forming full color-image from the CFA image by estimating missing band information is called image demosaicking (Li et al., 2008). One approach for low cost multispectral imaging system is the extension of CFA to MSFA. In the MSFA pattern more than three spectral bands are arranged and complete multispectral image is generated from an MSFA image using an interpolation method called multispectral image demosaicking (MSID). However, image demosaicking in multispectral domain is more difficult and challenging than for RGB images because of the highly sparse sampling of each spectral band. Further, the quality of the constructed multispectral images not only relies upon the demosaicking technique as well as on the MSFA design used to capture the MSFA image.

Many color image demosaicking methods have been proposed (Li et al., 2008; Menon and Menon, 2011), but all of these are restrained to RGB images only. The existing generic multispectral image demosaicking methods (Miao et al., 2006; Brauers and Aach, 2006; Aggarwal and Majumdar, 2014b) fail to generate good quality multispectral images, especially for higher band multispectral images. The other multispectral demosaicking methods (Mihoubi et al., 2017; Monno et al., 2015; Monno et al., 2012; Monno et al., 2011; Jaiswal et al., 2017) are restricted to a fixed number of spectral bands multispectral images.

The inspiration of this work is to propose an efficient and generic MSID approach as the requirement of the number of spectral bands is application-specific. This paper proposes an MSID method utilizing both the spatial and spectral correlation in the MSFA image. The proposed method uses the preferred binary-tree based MSFA patterns (Miao and Qi, 2006), which are considered most compact and designable for any number of bands in comparison to non-redundant MSFAs (Brauers and Aach, 2006) and uniform MSFAs (Aggarwal and Majumdar, 2014b). We design the filters based on the probability of appearance (PoA) of spectral bands in the MSFA image and use these PoA based filters to interpolate the subsampled bands of MSFA image to generate the complete multispectral image. To further improve the generated image's quality, we apply the spectral difference-based method using filters designed. Experimental results on multiple datasets show the efficacy of the proposed MSID method over the other state-of-the-art generic MSID methods, both quantitatively and visually.

The remainder of this paper is organized as follows. In section 2, the authors describe the related works on different MSFA patterns and corresponding MSID methods. In Section 3, the authors present the proposed method. Section 4 represents the experimental results. Finally, Section 5 presents conclusions and future work.

2 RELATED WORK

In this section, we discuss different MSFA patterns present in the literature and associated multispectral demosaicking methods. We divide the basic MSFA patterns into two categories based on the PoA of bands in MSFA: *(i)* Bands with equal PoA; and *(ii)* Bands with the different PoA.

2.1 MSFA with Equal PoA of Bands and Related MSID Methods

Many MSFA designs (Brauers and Aach, 2006; Mihoubi et al., 2015; Aggarwal and Majumdar, 2014b) with equal PoA of bands have been proposed for MSID. The work (Brauers and Aach, 2006) proposed a six-band non-redundant MSFA pattern as shown in Figure 1(g) which stores bands in 3×2 pattern. Brauers and Aach extended the color-difference-interpolation of CFA demosaicking to the multispectral domain. But it failed to generate quality multispectral images. Further, (Mizutani et al., 2014) improved Brauers and Aach method by iterating demosaicking method multiple times. The number of iterations depended on the correlation between two spectral bands. Later, (Brauers and Aach, 2006) is generalized for any K-band multispectral images (Gupta and Ram, 2019).

In (Mihoubi et al., 2015) authors proposed square-shaped non-redundant MSFA design patterns for 4, 9, and 16 bands multispectral images as shown in Figure

1(d). Here, the authors used the concept of panchromatic image (intensity image), which is strongly correlated with each band than bands considered pairwise. Further, Mihoubi et al. in (Mihoubi et al., 2017) had improved their previous work by proposing a new estimation of panchromatic image.

Aggarwal and Majumdar proposed two generic MSFA designs (Aggarwal and Majumdar, 2014b): (i) Uniform MSFA (Figure 1(c)) (ii) Random MSFA (Figure 1(f)). But on higher bands MSID, these designs are not practical because of their non-compact shape. In (Aggarwal and Majumdar, 2014b), authors used uniform MSFA for MSID and proposed a linear demosaicking method that requires the prior computation of parameters using original images. This limits the efficiency of the method as original images are not available in real-time. Wang et al. (Wang et al., 2014) proposed an MSID algorithm that was the combination of the linear minimum mean square error method and the residual interpolation algorithm (Kiku et al., 2013). Linear minimum mean square error is estimated between the reconstructed and original image using Wiener estimation. Later in the second step, residual interpolation is used to reduce the artifact of the reconstructed image. They used uniform MSFA in the demosaicking process, but their method is not MSFA design dependent.

2.2 MSFA with Different PoA of Bands and Related MSID Methods

In work (Miao and Qi, 2006), authors proposed a generic way to generate MSFA patterns using a binary tree for any number of bands multispectral images, as shown in Figure 1(a). Miao et al. in (Miao et al., 2006) introduced a binary tree-based edge sensing (BTES) generic method for MSID that used MSFA patterns formed using (Miao and Qi, 2006). BTES method uses the same binary tree for interpolation, which is used to create MSFA. It performs edge sensing interpolation to generate a complete multispectral image. In spite of the fact that BTES is generic, it doesn't perform well on a higher band multispectral images as it utilizes only spatial connection.

Binary-tree based MSFA patters are effectively utilized by several other methods (Monno et al., 2015; Monno et al., 2012; Monno et al., 2011; Monno et al., 2014; Wang et al., 2013a; Wang et al., 2013b). The methods (Monno et al., 2015; Monno et al., 2012; Monno et al., 2011; Monno et al., 2014) used a five-band MSFA pattern and kept PoA of G-band *0.5*, as shown in Figure 1(b). Monno et. al. (Monno et al., 2015; Monno et al., 2012; Monno et al., 2011; Monno et al., 2014) proposed several MSID methods based on proposed MSFA patterns. In (Monno et al., 2011), (Monno et al., 2012), and (Monno et al., 2014), authors adopted the idea of guide image (generated from under sampled G-band), and later they applied guide image as a reference image to interpolate remaining under-sampled bands based on (He et al., 2013). (Monno et al., 2011) extended existing upsampling methods to adaptive kernel upsampling methods applying an adaptive kernel to reconstruct each band and later improved in (Monno et al., 2012) using the guided filter. To further enhance (Monno et al., 2012), in (Monno et al., 2015), the authors used multiple guide images for interpolation. This approach is not practical for a higher band multispectral image. It is restricted to the MSFA pattern where G-band has PoA 0.5, making other bands severely undersampled in higher band multispectral image. (Jaiswal et al., 2017) also utilized the MSFA generated using (Monno et al., 2015) and proposed an adaptive spectral correlation based MSID method for five-band multispectral images. The proposed method uses high-frequency components of the G band to interpolate other bands using inter-band correlation analysis.

Few supervised learning-based MSID methods (Aggarwal and Majumdar, 2014b; Shopovska et al., 2018; Habtegebrial et al., 2019; Shoeiby et al., 2020) also had been introduced. However, these methods demanded the complete multispectral images for their models' learning/training parameters, which are not accessible in the real capturing situation. In (Aggarwal and Majumdar, 2014b), undersample bands are interpolated using linear filtering with the help of kernel. The parameters of the kernel are computed by applying the Winner estimation. In work (Shopovska et al., 2018), authors proposed 4-band MSID method based on residual U-Net (Ronneberger et al., 2015). In (Habtegebrial et al., 2019), a convolution neural network-based solution is proposed for image demosaicking. These algorithms are trained and tested on a similar dataset. This testing technique does not confirm the efficacy of introduced deep learning methods in the multispectral domain.

2.3 Our Considered MSFA Patterns

As the effectiveness of MSID methods also depends on the MSFA patterns, we use binary-tree based MSFA patters proposed by (Miao and Qi, 2006). The reason to use them is their compact design, which makes them suitable for MSID. There are many MSID methods (Monno et al., 2015; Monno et al., 2012; Monno et al., 2011; Monno et al., 2014; Wang et al., 2013a; Pearce et al., 2016; Jaiswal et al., 2017)

that have proven the efficacy of binary-tree based methods. We have shown our considered binary-tree based MSFA patterns in Figure 2.

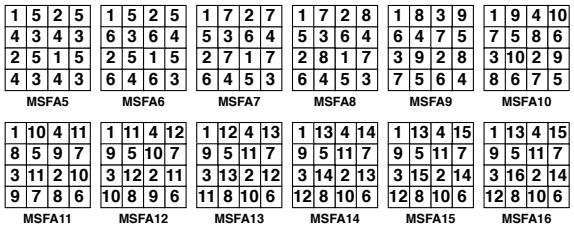

Figure 2: Binary-tree based MSFA design used for 5-16 band multispectral image demosaicking.

3 PROPOSED ALGORITHM

In this paper, we propose an MSID method, which utilizes both spatial and spectral correlation present in the MSFA image captured by a single camera. The proposed method can be extended to any K-band multispectral image. It uses binary-tree based MSFA pattern (Miao and Qi, 2006) to capture the initial mosaic image (MSFA image) which is later demosaicked using the proposed method to generate complete K-band multispectral image. Binary-tree based MSFA has the most compact shape as compared to non-redundant (Gupta and Ram, 2019) and uniform MSFA (Aggarwal and Majumdar, 2014a) pattern which makes it more efficient for the demosaicking process. The complete proposed demosaicking process includes two steps (as shown in Figure 3 (a)): (i) interpolate missing pixel values using a weighted bilinear approach and new filters proposed. This step utilizes only spatial correlation present in MSFA image and it is based on the PoA of each band in MSFA image; (ii) utilize spectral correlation present in the image using bilinear spectral difference to further improve the quality of image.

3.1 PoA based Convolution Filter based Weighted Bilinear

Brauers and Aach gave a filter which is used for weighted bilinear interpolation to interpolate 6-band MSFA image generated using non-redundant MSFA pattern. This technique is generalized by (Gupta and Ram, 2019) for non-redundant MSFA pattern. However, they also reported the weak performance of their generalized weighted bilinear method as these filters cannot be used to interpolate subsampled MSFA images generated using the compact MSFAs that are more preferred. Here, we propose filters based on

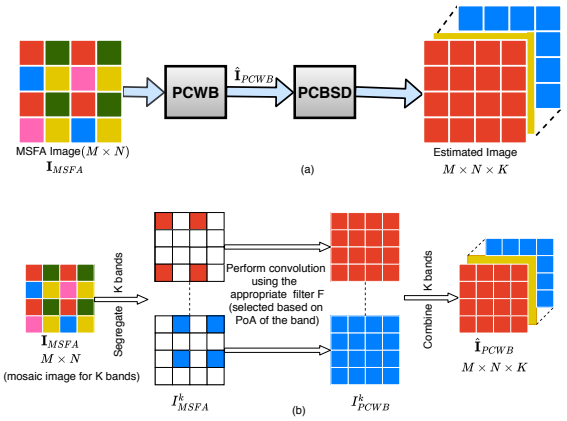

Figure 3: (a) Our proposed multispectral demosaicking method, (b) PoA based Convolution filter based Weighted Bilinear (PCWB).

PoA of bands in MSFA image and which are used to interpolate missing pixel values.

3.1.1 Filter Design based on PoA

Each spectral band in the MSFA image has a fixed PoA and it is pre-decided as per the MSFA design. To find the missing pixel values of any spectral band, we design a filter that depends on the PoA of that spectral band in the subsampled MSFA image. Later, we use these designed filters to generate a complete multispectral image. Let $B_M = \{b^1, \ldots b^K\}$ is a set of K binary masks, each of size $M \times N$, derived from the basic mosaic pattern; the binary mask b^k has value 1 only at locations where k^{th} band's original values are there in the input mosaic image, I^k_{MSFA} of size $M \times N$. To design a filter F that can be used to interpolate the missing pixel values of a band k in our convolution based weighted bilinear interpolation approach, the following properties shall be supported.

1. As the basic mosaic pattern is repeatedly tiled, horizontally and vertically, and accordingly the input mosaic images are generated by the image acquisition system, the convolution filter F must be symmetric. Considering the center pixel location of the filter to be $(0,0)$ and the filter F to be of size $(2p+1) \times (2p+1)$,
$$F(i,j) = F(-i,-j) \quad \forall i,j \in (-p,p) \qquad (1)$$
2. To interpolate band k at unknown location (x,y), it requires at least two known pixels values of band k in the neighborhood of location (x,y). As the band's PoA decreases, the filter size corresponding to that band must increase to accommodate the minimum required known pixel values for interpolation. For any spectral band with $PoA = \frac{1}{2^d}$,
$$p = max(1, d-1) \qquad (2)$$

3. The insight for this property is that - farther the known pixel value in the neighborhood of the unknown value, lesser shall be its weightage in estimating the unknown at center. Let (ix,iy) and (jx,jy) are two locations in the filter F, $if(dist(ix,iy) \geqslant dist(jx,jy))$,

$$F(ix,iy) \leqslant F(jx,jy) \tag{3}$$

where, *dist()* calculates spatial distance from the center (0,0).

4. We shall not interpolate or say, modify the (original) pixel values that have already been sensed. So, $F(0,0) = 1$ in order to retain the original value and to avoid the modification by any known pixel values that can be possibly present in the neighborhood of the center pixel considered, we shall have this filter property.

$$F(i,j) = 0 \quad \forall (i,j) \in \Omega_1 \tag{4}$$

where, Ω_1 is the set of those locations within the neighborhood of and in reference to the central pixel location (x,y) where $b^k(x,y) = 1$ and

$$\Omega_1 = \{(u,v) \mid -p \leqslant u,v \leqslant p, (u,v)! = (0,0) \text{ and } b^k(x-u,y-v) = 1\} \tag{5}$$

5. Consider now any specific location (x,y) where the pixel value is unknown. This missing value is aimed to be estimated using the weighted contributions from all the known pixel values in the neighborhood considered and the weights must be normalized. In reference to this location (x,y) where $b^k(x,y) = 0$, let us define set Ω_0 to be the set of those few locations within $(2p+1) \times (2p+1)$ neighborhood around center location (x,y) where the pixel values of that spectral band would be known, so

$$\Omega_0 = \{(u,v) \mid -p \leqslant u,v \leqslant p \text{ and } b^k(x-u,y-v) = 1\} \tag{6}$$

For every such location (x,y) where $b^k(x,y) = 0$ and the corresponding Ω_0, the following properties are to be considered:

$$F(i,j)! = 0 \quad \forall (i,j) \in \Omega_0 \tag{7}$$

and

$$\sum_{(i,j)\in\Omega_0} F(i,j) = 1 \tag{8}$$

It may appear that we have to explore all possible locations of the $M \times N$ size binary mask for each band for designing the filters; however, as the binary mask is prepared using the basic mosaic pattern that is tiled repeatedly, both horizontally and vertically, and the mosaic pattern is designed using binary tree based method, the number of possible configurations to be explored is 1/PoA. For example, let us consider band k whose PoA is $\frac{1}{8}$. In Figure 4, we show all possible pixel arrangements for band k w.r.t. the central pixel, where band k value has to be estimated in the image I^k_{MSFA}. Figure 4((a) - (g)) show the seven arrangements in which the band k value at center pixel location is unknown and Figure 4(h) shows the arrangement in which the band k value is already known at the center. Considering these all possible arrangements and the above mentioned properties, we construct convolution filter F_3, as shown in Figure 5, and we use this filter F_3 to interpolate the bands having PoA$\frac{1}{8}$, in our new approach as described in the next section. Similarly, by considering all pixels arrangement for bands having PoA $\frac{1}{2}$, $\frac{1}{4}$, and $\frac{1}{16}$, we design new filters F_1, F_2, and filter F_4, as shown in Figure 5, to interpolate bands having PoA $\frac{1}{2}$, $\frac{1}{4}$, and $\frac{1}{16}$, respectively.

3.1.2 Interpolation Algorithm

Here, we present PoA based convolution filter based weighted bilinear (PCWB) algorithm, where appropriate filter is selected for a band considering its PoA in the MSFA image. Presently, we consider upto 16-band multispectral images and the minimum PoA to be $\frac{1}{16}$. Accordingly, the algorithm is presented below. Also, the illustration of the interpolation process is shown in the Figure 3 (b).

Algorithm 1: PCWB.

Input: I_{MSFA}, $F1$, $F2$, $F3$, $F4$, B_M

For each band k repeat :

$I^k_{MSFA} = I_{MSFA} \odot b^k$

if (PoA(k) == 1/2)

$\hat{I}^k_{PCWB} = I^k_{MSFA} * (F1)$

else if (PoA(k) == 1/4)

$\hat{I}^k_{PCWB} = I^k_{MSFA} * (F2)$

else if (PoA(k) == 1/8)

$\hat{I}^k_{PCWB} = I^k_{MSFA} * (F3)$

else

$\hat{I}^k_{PCWB} = I^k_{MSFA} * (F4)$

where, I_{MSFA} is $M \times N$ size input mosaic image for K bands; $B_M = \{b^1, \ldots b^K\}$ is a set of K binary masks, each of size $M \times N$, derived from the basic mosaic pattern; $\{F_1, F_2, F_3, F_4\}$ is a set of filters used for interpolation; $'*'$ is Convolution operator; and '$\odot$' is element wise multiplication operator. The binary mask b^k has value 1 only at locations where k^{th} band's orig-

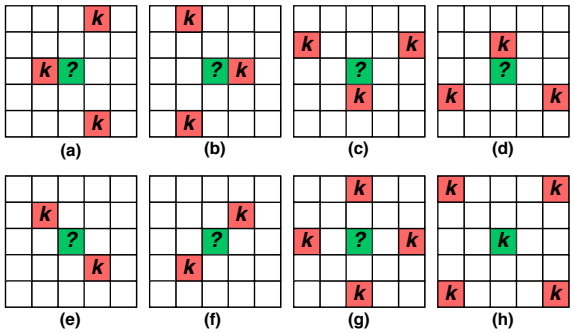

Figure 4: All possible pixel arrangements for k^{th} band having PoA = $\frac{1}{8}$ w.r.t. the central pixel in the binary tree based MSFAs. (a) - (g) The seven arrangements where k^{th} band value is not known at center (h) The arrangement where k^{th} band value is at center.

inal values are there. $\hat{I}^k_{PCWB}$ is interpolated k^{th} band. Image $\hat{\mathbf{I}}_{PCWB}$ is generated by combining all interpolated K-bands.

This algorithm is currently presented for upto 16-band multispectral images but the appropriate filters can be designed as per the properties discussed earlier and the algorithm can then be easily extended further for large number of bands size multispectral images.

$$F_1 = (1/2)\begin{bmatrix} 0 & 0.5 & 0 \\ 0.5 & 2 & 0.5 \\ 0 & 0.5 & 0 \end{bmatrix}; \quad F_2 = (1/4)\begin{bmatrix} 1 & 2 & 1 \\ 2 & 4 & 2 \\ 1 & 2 & 1 \end{bmatrix};$$

$$F_3 = (1/8)\begin{bmatrix} 0 & 2 & 2 & 2 & 0 \\ 2 & 4 & 4 & 4 & 2 \\ 2 & 4 & 8 & 4 & 2 \\ 2 & 4 & 4 & 4 & 2 \\ 0 & 2 & 2 & 2 & 0 \end{bmatrix}; \quad F_4 = (1/16)\begin{bmatrix} 1 & 2 & 3 & 4 & 3 & 2 & 1 \\ 2 & 4 & 6 & 8 & 6 & 4 & 2 \\ 3 & 6 & 9 & 12 & 9 & 6 & 3 \\ 4 & 8 & 12 & 16 & 12 & 8 & 4 \\ 3 & 6 & 9 & 12 & 9 & 6 & 3 \\ 2 & 4 & 6 & 8 & 6 & 4 & 2 \\ 1 & 2 & 3 & 4 & 3 & 2 & 1 \end{bmatrix};$$

Figure 5: Convolution Filters designed for PCWB.

3.2 PoA based Convolution Filter based Bilinear Spectral Difference

To further improve the quality of image generated using PCWB, we present PoA based convolution filter based bilinear spectral difference (PCBSD) method. The PCBSD method is applicable for binary-tree based MSFAs and thus generalized to interpolate any K-band images. It is motivated from color difference based approach (Brauers and Aach, 2006). Using $\hat{\mathbf{I}}_{PCWB}$ as the initial multispectral image, the following steps are performed to generate a final interpolated multispectral image $\hat{\mathbf{I}}$.

1. For each ordered pair (p,q) of bands, determine the sparse band difference $\tilde{D}^{pq}$ at q^{th} band's locations.

$$I^q_{MSFA} = I_{MSFA} \odot b^q \tag{9}$$

$$\tilde{D}^{pq} = \hat{I}^p_{PCWB} \odot b^q - I^q_{MSFA} \tag{10}$$

2. Now compute the fully-defined band difference $\hat{D}^{pq}$ using PCWB interpolation of $\tilde{D}^{pq}$.
3. For each band q, estimate $\hat{I}^q$ at pixel locations where $b^p(x,y) = 1$ as:

$$\hat{I}^q = \sum_{p=1}^{K} \left(I^p_{MSFA} - \hat{D}^{pq} \odot b^p\right) \tag{11}$$

Now, all K bands are fully-defined and together form the complete multispectral image $\hat{\mathbf{I}}$.

4 EXPERIMENTAL RESULTS

4.1 Datasets

We examine the performance of the proposed method (PCBSD) on different datasets and compare it with different state-of-the-art methods. To evaluate different multispectral image demosaicking methods, we use two publicly available multispectral image datasets, the Cave dataset (Yasuma et al., 2010) and the TokyoTech dataset (Monno et al., 2015). The Cave dataset contains 31-band images of 31 scenes and these bands range from 400nm to 700nm with a spectral gap of 10nm. The TokyoTech dataset includes 30 images. Each image has 31-bands, and the spectral range of these 31-bands is from 420nm to 720nm with a spectral gap of 10nm. Each image is of size 512×512 in the Cave dataset and 500×500 in the TokyoTech dataset.

4.2 Quantitative Comparison

We compare different MSID methods on multispectral images with band size (K) varying from 5 to 16. To simulate the K-band ground truth multispectral images, we select K-bands at equal spectral gaps starting from the first band of the 31-band multispectral images. Then, we perform the mosaicking and demosaicking process to generate the K-band multispectral image. The demosaicked K-band image is compared with the ground truth multispectral image for quality assessment. We compare the proposed method with other existing generic MSID methods: WB (Gupta and Ram, 2019), SD (Brauers and Aach, 2006), LMSD (Aggarwal and Majumdar, 2014b), ISD (Mizutani et al., 2014) and BTES (Miao et al., 2006). To compare the estimated image's quality with

Table 1: Comparison of different MSID methods based on PSNR on the different datasets (K denotes number of bands). There are a few other MSID methods (Monno et al., 2015; Mihoubi et al., 2017; Jaiswal et al., 2017) as well, but these are specific to one band only and therefore not considered for comparison.

	TokyoTech							Cave						
K	**WB**	**SD**	**BTES**	**LMSD**	**ISD**	**PCWB**	**PCBSD**	**WB**	**SD**	**BTES**	**LMSD**	**ISD**	**PCWB**	**PCBSD**
5	32.27	33.29	36.79	35.61	33.13	36.92	**37.25**	34.45	35.36	39.23	**40.10**	35.23	39.18	39.21
6	35.56	36.37	35.68	33.30	35.55	35.70	**36.54**	37.26	38.16	38.22	**38.65**	37.65	38.00	38.57
7	29.79	29.21	34.96	32.72	30.85	34.92	**36.01**	32.31	32.62	37.68	**38.35**	33.50	37.39	38.33
8	33.49	34.69	34.58	31.43	34.19	34.51	**35.78**	35.31	36.71	37.17	37.30	36.59	36.85	**38.22**
9	34.12	35.35	33.99	25.11	34.58	34.01	**35.44**	36.00	37.51	36.67	29.58	37.20	36.41	**37.99**
10	31.91	33.26	33.24	30.36	33.14	33.29	**34.74**	33.95	35.54	35.87	36.26	35.67	35.70	**37.42**
11	27.19	28.20	32.56	24.40	28.28	32.64	**34.12**	29.70	31.05	35.23	28.86	31.36	35.13	**36.81**
12	32.76	34.35	32.30	25.21	33.92	32.70	**34.45**	34.66	36.48	34.68	28.95	36.61	34.88	**36.91**
13	26.69	27.63	31.61	24.58	27.95	32.24	**33.99**	29.03	30.50	34.16	28.67	31.10	34.50	**36.49**
14	29.78	31.22	31.67	24.32	31.46	31.81	**33.67**	32.04	33.80	34.17	28.38	34.30	34.15	**36.17**
15	31.15	32.64	31.28	24.02	32.63	31.42	**33.21**	33.38	35.08	33.88	28.26	35.43	33.89	**35.76**
16	31.06	32.65	30.92	23.85	32.37	31.06	**32.96**	33.71	35.45	33.67	28.13	35.57	33.70	**35.60**
Avg	31.31	32.41	33.30	27.91	32.34	33.43	**34.85**	33.48	34.85	35.89	32.62	35.02	35.82	**37.29**

Table 2: Comparison of different MSID methods based on SSIM on the different datasets. (K denotes number of bands).

	TokyoTech							Cave						
K	**WB**	**SD**	**BTES**	**LMSD**	**ISD**	**PCWB**	**PCBSD**	**WB**	**SD**	**BTES**	**LMSD**	**ISD**	**PCWB**	**PCBSD**
5	0.9276	0.9367	0.9739	0.9623	0.9361	**0.9793**	0.9788	0.9620	0.9647	0.9869	0.9864	0.9634	**0.9880**	0.9845
6	0.9682	0.9737	0.9645	0.9474	0.9734	0.9713	**0.9756**	0.9816	0.9833	0.9826	0.9809	0.9829	**0.9837**	0.9828
7	0.8848	0.8821	0.9584	0.9314	0.9018	0.9661	**0.9731**	0.9380	0.9379	0.9799	0.9778	0.9440	0.9810	**0.9826**
8	0.9471	0.9601	0.9538	0.9123	0.9621	0.9624	**0.9718**	0.9690	0.9776	0.9777	0.9716	0.9791	0.9789	**0.9832**
9	0.9570	0.9653	0.9465	0.7876	0.9642	0.9557	**0.9687**	0.9752	0.9809	0.9745	0.9044	0.9809	0.9761	**0.9816**
10	0.9253	0.9464	0.9373	0.8880	0.9525	0.9478	**0.9643**	0.9583	0.9707	0.9695	0.9611	0.9737	0.9714	**0.9791**
11	0.8189	0.8435	0.9286	0.7549	0.8441	0.9402	**0.9596**	0.8987	0.9103	0.9648	0.8837	0.9080	0.9670	**0.9763**
12	0.9372	0.9555	0.9250	0.7668	0.9572	0.9367	**0.9625**	0.9645	0.9762	0.9631	0.8788	0.9778	0.9655	**0.9788**
13	0.7982	0.8294	0.9186	0.7422	0.8345	0.9315	**0.9591**	0.8864	0.9015	0.9597	0.8738	0.8980	0.9624	**0.9767**
14	0.8852	0.9208	0.9141	0.7258	0.9338	0.9269	**0.9569**	0.9362	0.9567	0.9568	0.8615	0.9615	0.9596	**0.9755**
15	0.9149	0.9394	0.9091	0.7151	0.9454	0.9226	**0.9540**	0.9521	0.9673	0.9541	0.8595	0.9707	0.9571	**0.9737**
16	0.9184	0.9349	0.9041	0.7107	0.9340	0.9182	**0.9514**	0.9547	0.9668	0.9515	0.8503	0.9677	0.9547	**0.9725**
Avg	0.9069	0.9240	0.9362	0.8204	0.9283	0.9466	**0.9647**	0.9480	0.9578	0.9684	0.9158	0.9590	0.9704	**0.9789**

Table 3: PSNR values of sRGB images generated by different MSID methods on the TokyoTech and Cave datasets.

	TokyoTech							Cave						
K	**WB**	**SD**	**BTES**	**LMSD**	**ISD**	**PCWB**	**PCBSD**	**WB**	**SD**	**BTES**	**LMSD**	**ISD**	**PCWB**	**PCBSD**
5	32.48	33.56	37.83	35.77	33.52	38.05	**38.52**	33.56	34.77	38.32	39.31	34.84	38.15	**40.04**
6	35.51	**36.41**	34.90	32.87	35.67	34.80	36.39	38.00	39.71	38.57	39.47	39.33	38.28	**40.18**
7	30.72	29.30	35.87	33.60	31.79	35.92	**37.14**	32.93	32.76	38.22	38.97	34.35	37.97	**39.85**
8	35.14	36.35	36.48	32.46	35.79	36.64	**37.76**	36.74	38.53	38.76	38.31	38.47	38.56	**40.33**
9	36.09	37.41	35.83	26.15	36.33	36.15	**37.65**	37.61	39.76	38.29	30.46	39.14	38.16	**40.86**
10	33.88	35.25	35.32	31.36	34.95	35.72	**36.90**	35.83	37.74	37.92	37.38	37.74	37.98	**39.99**
11	28.64	29.56	34.41	25.76	29.66	34.87	**36.06**	30.47	31.95	36.81	29.88	32.26	37.01	**39.34**
12	35.05	36.84	34.81	26.47	35.77	35.57	**37.29**	37.27	39.72	37.33	30.50	39.25	38.03	**40.86**
13	27.93	28.91	33.87	25.66	29.15	34.74	**36.72**	30.06	31.67	36.37	29.78	32.20	37.28	**40.07**
14	31.92	33.52	33.49	25.41	33.38	34.19	**36.40**	33.88	36.03	36.12	29.42	36.11	36.62	**39.55**
15	33.80	35.39	33.38	25.21	34.74	34.09	**36.12**	35.66	37.94	35.85	29.33	37.65	36.40	**39.09**
16	33.31	34.82	33.37	25.07	34.28	34.08	**36.05**	35.70	37.97	35.82	29.29	37.66	36.38	**39.03**
Avg	32.87	33.94	34.96	28.82	33.75	35.40	**36.92**	34.81	36.55	37.37	33.51	36.58	37.57	**39.93**

the original image, we evaluate these methods based on the PSNR and SSIM image quality metrics.

Tables 1 and 2 show the quantitative performance of our proposed method on different band's multispectral images taken from the TokyoTech and Cave datasets under CIE D65 illumination. WB and BTES methods have given poor performance, especially on higher band images, because they only utilize spatial correlation presents in the image. SD and ISD methods perform better than the BTES method on 6, 8, 9, 12, 15, and 16 bands multispectral images. However, the BTES method, using compact (binary-tree based) MSFAs, performs better for some bands such as 5, 7, 11, and 13. The sharp drop in the performance for the 5, 7, 11, and 13 band images in WB, SD, and ISD methods is because of the non-compact aspect of the non-redundant MSFAs used in these methods. This observation was the motivation for the proposed method. The proposed method PCBSD performs better than the other methods on the Cave and

Table 4: SSIM values of sRGB images generated by different MSID methods on the TokyoTech and Cave datasets.

	TokyoTech							Cave						
K	**WB**	**SD**	**BTES**	**LMSD**	**ISD**	**PCWB**	**PCBSD**	**WB**	**SD**	**BTES**	**LMSD**	**ISD**	**PCWB**	**PCBSD**
5	0.9275	0.9380	0.9770	0.9557	0.9377	**0.9822**	0.9809	0.9527	0.9615	0.9827	0.9813	0.9609	0.9830	**0.9876**
6	0.9673	**0.9735**	0.9562	0.9376	0.9733	0.9636	0.9717	0.9802	**0.9863**	0.9793	0.9769	0.9861	0.9799	0.9856
7	0.8866	0.8674	0.9595	0.9213	0.9034	0.9673	**0.9727**	0.9364	0.9334	0.9792	0.9748	0.9467	0.9803	**0.9864**
8	0.9537	0.9660	0.9631	0.9092	0.9667	0.9716	**0.9776**	0.9731	0.9824	0.9814	0.9707	0.9834	0.9828	**0.9880**
9	0.9682	0.9741	0.9569	0.7931	0.9701	0.9674	**0.9766**	0.9795	0.9869	0.9800	0.9005	0.9852	0.9821	**0.9897**
10	0.9392	0.9569	0.9506	0.8880	0.9599	0.9625	**0.9716**	0.9660	0.9783	0.9762	0.9608	0.9793	0.9791	**0.9861**
11	0.8326	0.8545	0.9394	0.7632	0.8547	0.9531	**0.9650**	0.8997	0.9136	0.9714	0.8844	0.9105	0.9752	**0.9839**
12	0.9564	0.9689	0.9453	0.7763	0.9636	0.9597	**0.9750**	0.9742	0.9852	0.9752	0.8814	0.9828	0.9795	**0.9894**
13	0.8126	0.8421	0.9359	0.8583	0.8454	0.9530	**0.9719**	0.8880	0.9059	0.9705	0.8735	0.9014	0.9761	**0.9875**
14	0.9096	0.9384	0.9297	0.7360	0.9443	0.9482	**0.9701**	0.9470	0.9668	0.9662	0.8611	0.9667	0.9724	**0.9862**
15	0.9409	0.9569	0.9285	0.7263	0.9558	0.9473	**0.9689**	0.9657	0.9789	0.9644	0.8603	0.9774	0.9710	**0.9848**
16	0.9396	0.9491	0.9284	0.7202	0.9437	0.9471	**0.9680**	0.9660	0.9771	0.9642	0.8536	0.9745	0.9709	**0.9845**
Avg	0.9195	0.9322	0.9475	0.8321	0.9349	0.9603	**0.9725**	0.9524	0.9630	0.9742	0.9149	0.9629	0.9777	**0.9866**

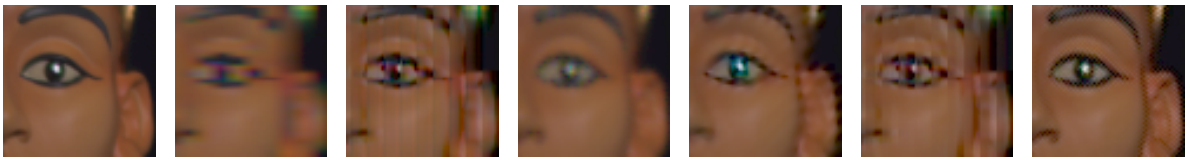

(a_1) Cropped (a_2) WB (a_3) SD (a_4) BTES (a_5) LMSD (a_6) ISD (a_7) PCBSD

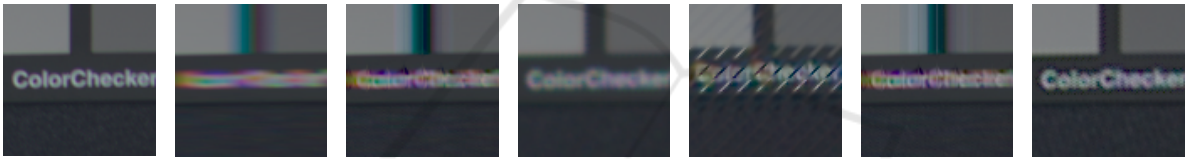

(b_1) Cropped (b_2) WB (b_3) SD (b_4) BTES (b_5) LMSD (b_6) ISD (b_7) PCBSD

Figure 6: Visual comparison of demosaicked images (sRGB) generated from the 7 and 11 bands multispectral images.

the TokyoTech datasets for both the metrics PSNR and SSIM. Although LMSD performs better on a few band multispectral images, it uses the same dataset's original images for parameter computations but in real world situation, the original completed images won't be available for the MSFA based multispectral camera and the parameters cannot be therefore computed for that device. Some of the recent methods are not considered in comparison as unlike the proposed method, they were not applicable to several different band-size multispectral images. Overall, the proposed method provides the improvement by 1.55dB and 1.4 dB in PSNR over the second best performing generic method - BTES, for the TokyoTech and Cave datasets, respectively. In terms of SSIM also, an improvement of around 3% and 1% is observed in comparison to BTES.

Table 2 presents the SSIM performance comparison of the different MSID methods for both datasets. The SSIM model is consistent with our visual perception. SSIM value close to 1 indicates that the demosaicked image is similar to the ground truth image. The proposed method produces a higher SSIM in almost all K-band multispectral images for both datasets.

To estimate colorimetric correctness, we convert the K-band multispectral images into the sRGB domain. To convert into the sRGB domain, we calculate spectral reflectance images from the demosaicked K-band multispectral images and convert the reflectance images to sRGB images using xyz color matching functions (Monno et al., 2015). Table 3 and Table 4 show the PSNR and SSIM values of sRGB images generated by different MSID methods on both datasets. Clearly, the sRGB images generated from the proposed method have the highest PSNR and SSIM values among all methods.

4.3 Visual Comparison

Figure 6 shows the visual comparison of the sRGB images generated by the different MSID methods for 7-band and 11-band multispectral images. We select smaller portions from multiple sRGB images so that artifacts should be visible. We can observe that other existing MSID methods generate significant artifacts, whereas our proposed method reproduces the sRGB images more accurately than the other MSID methods.

5 CONCLUSIONS

Non-redundant MSFAs are generally non-compact, which reduce the potency of MSID methods. The binary-tree based MSFAs are compact and can be designed for any-band multispectral images. However, for these compact MSFAs, the existing demosaicking methods are either limited in performance or in generalizability. In this work, we have designed new convolution filters based on PoA of the bands in the binary-tree based MSFAs, and based on these filters, we proposed a novel PoA based convolution filter based weighted bilinear interpolation (PCWB) approach. By generalizing the color difference technique, we finally presented the new approach, PoA based convolution filter based spectral difference method (PCBSD) that relies on PCWB for providing the first estimate and also for estimating the spectral differences, and thus PCWB is further improvised. The new method, PCBSD, is efficient and can be effectively used for any K-band multispectral image. Experimental results showed that proposed MSID methods outperform the exiting generic MSID methods based on quantitative (PSNR and SSIM) and visual comparison both on two publically available datasets. In the future, we plan to extend this convolution filter approach to extend other image demosaicking methods, and we plan to explore the performance of the proposed method in the context of applications of multispectral imaging.

ACKNOWLEDGEMENTS

This research is supported by the DST Science and Engineering Research Board, India under grant ECR/2017/003478.

REFERENCES

Aggarwal, H. K. and Majumdar, A. (2014a). Compressive sensing multi-spectral demosaicing from single sensor architecture. In *Proceedings of IEEE China Summit International Conference on Signal and Information Processing*, pages 334–338.

Aggarwal, H. K. and Majumdar, A. (2014b). Single-sensor multi-spectral image demosaicing algorithm using learned interpolation weights. In *Proceedings of the International Geoscience and Remote Sensing Symposium*, pages 2011–2014.

Brauers, J. and Aach, T. (2006). A color filter array based multispectral camera. In *12. Workshop Farbbildverarbeitung*, pages 55–64.

Chen, I. and Lin, H. (2020). Detection, counting and maturity assessment of cherry tomatoes using multi-spectral images and machine learning techniques. In *Proceedings of International Joint Conference on Computer Vision, Imaging and Computer Graphics Theory and Applications(VISIGRAPP)*, pages 759–766.

Chi, C., Yoo, H., and Ben-Ezra, M. (2010). Multi-spectral imaging by optimized wide band illumination. *International Journal of Computer Vision*, 86(2-3):. 140–151.

Fukuda, H., Uchiyama, T., Haneishi, H.and Yamaguchi, M., and Ohyama, N. (2005). Development of 16-band multispectral image archiving system. In *Proceedings of SPIE*, pages 136–145.

Geelen, B., Tack, N., and Lambrechts, A. (2014). A compact snapshot multispectral imager with a monolithically integrated per-pixel filter mosaic. In *Proceedings of SPIE*, volume 8974, page 89740L.

Gupta, M. and Ram, M. (2019). Weighted bilinear interpolation based generic multispectral image demosaicking method. *Journal of Graphic Era University*, 7(2):108–118.

Habtegebrial, T. A., Reis, G., and Stricker, D. (2019). Deep convolutional networks for snapshot hypercpectral demosaicking. In *10th Workshop on Hyperspectral Imaging and Signal Processing: Evolution in Remote Sensing*, pages 1–5.

He, K., Sun, J., and Tang, X. (2013). Guided image filtering. *IEEE Transactions on Pattern Analysis and Machine Intelligence*, 35(6):1397–1409.

Jaiswal, S. P., Fang, L., Jakhetiya, V., Pang, J., Mueller, K., and Au, O. C. (2017). Adaptive multispectral demosaicking based on frequency-domain analysis of spectral correlation. *IEEE Transactions on Image Processing*, 26(2):953–968.

Junior, J. D., Backes, A. R., and Escarpinati, M. C. (2019). Detection of control points for uav-multispectral sensed data registration through the combining of feature descriptors. In *Proceedings of International Joint Conference on Computer Vision, Imaging and Computer Graphics Theory and Applications(VISIGRAPP)*, pages 444–451.

Kiku, D., Monno, Y., Tanaka, M., and Okutomi, M. (2013). Residual interpolation for color image demosaicking. In *Proceedings of IEEE International Conference on Image Processing*, page 2304–2308.

Li, X., Gunturk, B., and Zhang, L. (2008). Image demosaicing: A systematic survey. *Proceedings of SPIE*, 6822:1–15.

Liu, C., Liu, W., Lu, X., Ma, F., Chen, W.and Yang, J., and Zheng, L. (2014). Application of multispectral imaging to determine quality attributes and ripeness stage in strawberry fruit. *PLoS ONE*, 9(2):1–8.

MacLachlan, A., Roberts, G., Biggs, E., and Boruff, B. (2017). Subpixel land-cover classification for improved urban area estimates using landsat. *International Journal of Remote Sensing*, 38(20):5763–5792.

Martinez, M. A., Valero, E. M., Hernández-Andrés, J., Romero, J., and Langfelder, G. (2014). Combining transverse field detectors and color filter arrays to im-

prove multispectral imaging systems. *Applied Optics*, 53(13):C14–C24.

Menon, D. and Menon, G. (2011). Color image demosaicking: An overview. *Signal Processing: Image Communication*, 26(8-9):518–533.

Miao, L. and Qi, H. (2006). The design and evaluation of a generic method for generating mosaicked multispectral filter arrays. *IEEE Transactions on Image Processing*, 15(9):2780–2791.

Miao, L., Ramanath, R., and Snyder, W. E. (2006). Binary tree-based generic demosaicking algorithm for multispectral filter arrays. *IEEE Transactions on Image Processing*, 15(11):3550–3558.

Mihoubi, S., Losson, O., Mathon, B., and Macaire, L. (2015). Multispectral demosaicking using intensity-based spectral correlation. In *Proceedings of the 5th International Conference on Image Processing Theory, Tools and Applications*, pages 461–466.

Mihoubi, S., Losson, O., Mathon, B., and Macaire, L. (2017). Multispectral demosaicing using pseudo-panchromatic image. *IEEE Transactions on Computational Imaging*, 3(4):982–995.

Mizutani, J., Ogawa, S., Shinoda, K., Hasegawa, M., and Kato, S. (2014). Multispectral demosaicking algorithm based on inter-channel correlation. In *Proceedings of the IEEE Visual Communications and Image Processing Conference*, pages 474–477.

Monno, Y., Kiku, D., Kikuchi, S., Tanaka, M., and Okutomi, M. (2014). Multispectral demosaicking with novel guide image generation and residual interpolation. In *Proceedings of IEEE International Conference on Image Processing*, pages 645–649.

Monno, Y., Kikuchi, S., Tanaka, M., and Okutomi, M. (2015). A practical one-shot multispectral imaging system using a single image sensor. *IEEE Transactions on Image Processing*, 24(10):3048–3059.

Monno, Y., Tanaka, M., and Okutomi, M. (2011). Multispectral demosaicking using adaptive kernel upsampling. In *Proceedings of IEEE International Conference on Image Processing*, pages 3157–3160.

Monno, Y., Tanaka, M., and Okutomi, M. (2012). Multispectral demosaicking using guided filter. In *Proceedings of the SPIE Electronic Imaging Annual Symposium*, pages 82990O–1–82990O–7.

Ohsawa, K., Ajito, T., Komiya, Y.and Fukuda, H., Haneishi, H., Yamaguchi, M., and Ohyama, N. (2004). Six band hdtv camera system for spectrum-based color reproduction. *Journal of Imaging Science and Technology*, 48(2):85–92.

Pearce, A. K., Fuchs, A., Fletcher, N., and Thurecht, K. (2016). Targeting nanomedicines to prostate cancer: evaluation of specificity of ligands to two different receptors in vivo. *Pharmaceutical Research*, 33(10):2388–2399.

Pichette, J., Laurence, A., Angulo, L., Lesage, F., Bouthillier, A., Nguyen, D., and Leblond, F. (2016). Intraoperative video-rate hemodynamic response assessment in human cortex using snapshot hyperspectral optical imaging. *Neurophotonics*, 3(4):045003.

Qin, J., Chao, K., Kim, M. S., Lu, R., and Burks, T. F. (2013). Hyperspectral and multi spectral imaging for evaluating food safety and quality. *Journal of Food Engineering*, 118(2):157–171.

Ronneberger, O., Fischer, P., and Brox, T. (2015). U-net: Convolutional networks for biomedical image segmentation. In *International Conference on Medical Image Computing and Computer-Assisted Intervention (MICCAI)*, page 234–241.

Shoeiby, M., Armin, M. A., Aliakbarian, S., Anwar, S., and Petersson, L. (2020). Mosaic super-resolution via sequential feature pyramid networks. In *Proceedings of Computer Vision and Pattern Recognition Workshops (CVPRW)*, pages 378– 387.

Shopovska, I., Jovanov, L., and Philips, W. (2018). Rgb-nir demosaicing using deep residual u-net. In *26th Telecommunications Forum*, pages 1–4.

Shrestha, R., Hardeberg, Y., and Mansouri, A. (2011). One-shot multispectral color imaging with a stereo camera. In *Proceedings of SPIE*, volume 7876, page 787609.

Thomas, J.-B., Lapray, P.-J., Gouton, P., and Clerc, C. (2016). Spectral characterization of a prototype sfa camera for joint visible and nir acquisition. *Sensor*, 16:993.

Tsuchida, M., Kawanishi, T., Kashino, K., and Yamato, J. (2012). A stereo nine-band camera for accurate color and spectrum reproduction. In *ACM SIGGRAPH 2012 Posters*, page 18.

Vayssade, J., Jones, G., Paoli, J., and Gee, C. (2020). Two-step multi-spectral registration via key-point detector and gradient similarity: Application to agronomic scenes for proxy-sensing. In *Proceedings of International Joint Conference on Computer Vision, Imaging and Computer Graphics Theory and Applications(VISIGRAPP)*, pages 103–110.

Wang, C., Wang, X., and Hardeberg, J. (2014). A linear interpolation algorithm for spectral filter array demosaicking. In *Proceedings of International Conference on Image and Signal Processing*, volume 8509, pages 151–160.

Wang, X., Thomas, J. B., Hardeberg, J. Y., and Gouton, P. (2013a). Discrete wavelet transform based multispectral filter array demosaicking. In *Proceedings of the Colour and Visual Computing Symposium*, pages 1–6.

Wang, X., Thomas, J.-B., Hardeberg, J. Y., and Gouton, P. (2013b). Median filtering in multispectral filter array demosaicking. In *Proceedings of SPIE*, volume 8660, page 86600E.

Yasuma, F., Mitsunaga, T., Iso, D., and Nayar, S. (2010). Generalized assorted pixel camera: Postcapture control of resolution, dynamic range, and spectrum. *IEEE Transactions on Image Processing*, 19(9):2241–2253.

Zenteno, O., Treuillet, S., and Lucas, Y. (2019). 3d cylinder pose estimation by maximization of binary masks similarity: A simulation study for multispectral endoscopy image registration. In *Proceedings of International Joint Conference on Computer Vision, Imaging and Computer Graphics Theory and Applications(VISIGRAPP)*, pages 857–864.

Zia, A., Liang, J., and Zhou, J.and Gao, Y. (2015). 3d reconstruction from hyperspectral images. In *Proceedings of IEEE Winter Conference on Applications of Computer Vision (WACV)*, page 318–325.